International Journal of Innovative Computing, Information and Control
Volume **9**, Number **2**, February **2013**

ICIC International ©2013 ISSN 1349-4198
pp. **841–849**

AN ADAPTIVE SQUARED GRADIENT ALGORITHM FOR AUTOFOCUSING OF THERMAL CAMERAS

Murat Selek

Department of Electronic Telecommunication Technology
Higher School of Vocational and Technical Sciences
Selcuk University
Konya 42003, Turkey
mselek@selcuk.edu.tr

Received January 2012; revised May 2012

Abstract. *The aim of this study is to select from the autofocusing algorithms developed for visible image devices such an algorithm that is the most successful for thermal image devices. For this purpose, 500 different thermal images were processed by the widely used autofocusing algorithms such as Variance, Autocorrelation, Brenner and Squared Gradient, and the average rate of successful autofocusing for each algorithm was determined. From these results, it was derived that the best performance for thermal images is provided by the Squared Gradient algorithm. The analysis of the results of experiments showed that the success of the Squared Gradient algorithm is significantly affected by the resolution of the thermal images. Therefore, we developed this algorithm so that it can be adaptive to the resolution of the thermal image camera to be autofocused. Due to this improvement, the average rate of successful autofocusing for thermal images has been increased from 87 to 96 percent.*
Keywords: Autofocusing, Image resolution, Focal plane, Thermal image

1. **Introduction.** The problem of *autofocusing* of digital image cameras becomes more and more important with rapid development of digital imaging systems [1-4]. To solve this problem, two types of autofocusing techniques called *active autofocusing* and *passive autofocusing* are used [1,3,5].

The active autofocusing technique emits ultrasonic or infrared electromagnetic waves and determines the correct focus by measuring the reflections of these waves from the surface of the imaged object [1,3,5]. This technique is fast since it requires taking only a single image from the object. Therefore, it can be utilized for real time applications [6,7]. Unfortunately, this technique might not yield good results for objects with different depths and reflecting surfaces [6,8]. Moreover, active autofocusing technique is highly costly and it requires high power consumption [1,3].

The passive autofocusing technique does not measure the distance between the object and the camera. It performs the autofocusing by exploiting various features of the image being taken [1,3,5]. The passive autofocusing technique-based algorithms are divided into four groups [1,8-12]: *derivative-based* [1-3,8-14], *statistics-based* [1,10-12], *histogram-based* [10,12,13] and *intuitive-based* [5,6,10-12] algorithms.

It is well known that the *contrast* between neighboring pixels of an image increases with the increase of the high-frequency content of the image [1,2,10]. That is, the neighboring pixels in images with high-frequency content have large differences in terms of intensity. Consequently, the larger these intensity differences in an image are, the sharper the edges of the image [1,2,10] become.

The *derivative-based* algorithms use the fact that an image at the focus has more high-frequency content than defocused images [10]. In these algorithms, to calculate the magnitudes of derivate vectors, the methods such as *Threshold Absolute Gradient*, *Squared Gradient*, *Brenner Gradient*, *Tenenbaum Gradient*, *Sum Of Modified Laplace*, *Energy Laplace* and *Wavelet* are used [1-3,6,9-11,14]. Unfortunately, these methods are highly sensitive to high-frequency noise.

The *statistics-based* algorithms use methods such as *Variance*, *Normalized Variance* and *Correlation*. These methods are much less sensitive to high-frequency noise than the *derivative-based* ones [1,10,11]. Although this feature constitutes an advantage in terms of image clarity, the ability to capitalize on the edge sharpness arising from intensity differences between the high-frequency pixels of these algorithms significantly decreases.

The *histogram-based* algorithms utilize the histogram of the pixels of an image to analyze the frequency and distribution of intensities of the pixels [10,12,13]. Yet, the focusing capability of the *histogram-based* algorithms is significantly lower than the others because they do not take into account the intensity differences between the pixels.

In the *intuitive-based* algorithms, a threshold for the gray level is determined. To obtain the maximal focus value, the count of the pixels with gray levels either above or below this threshold is used [5,6,10]. Nevertheless, the focusing capability of *intuitive-based* algorithms is even lower than that of the *histogram-based* algorithms because they do not take into account the intensity differences between the pixels.

The autofocusing algorithms explained above have been developed for visible imaging devices. However, unfortunately, despite the frequent use of the thermal image devices in many fields such as quality control in production environments, process monitoring, nondestructive testing, research and development of new products, condition monitoring and surveillance, predictive maintenance, military and medicine, there are no autofocusing algorithms for these devices. Moreover, there are no studies evaluating the behavior of existing autofocusing algorithms for thermal image devices.

In this study, the autofocusing algorithms such as *Squared Gradient Algorithm (SGA)*, *Brenner Algorithm (BA), Variance Algorithm (VA)* and *Autocorrelation Algorithm (AA)* were applied to 500 thermal images and the autofocusing performances of these algorithms were evaluated. The results given in Table 4 show that in terms of autofocusing of thermal images, the *SGA*, *BA*, *VA* and *AA* algorithms have success rates of 87%, 84%, 67% and 33%, respectively. According to these results, the SGA stands out as the most successful autofocusing algorithm for thermal images. In addition, these results demonstrate that this algorithm has produced varying performance of autofocusing depending on the resolution of the thermal camera and this performance can be increased by using a gap k obtained for each given resolution. This allows us to adapt the SGA to the resolution of the thermal image camera by adjusting the value of k. Therefore, in this study we mainly focus on the problem of the effect of the resolution of an image to the detection of its edges and on the problem of obtaining such a value for k that provides the best focusing for the given object. Therefore, the SGA improved in this study is referred to as *Adaptive SGA* (*ASGA*). The rest of this study is comprised of the following sections: Section 2 deals with the problem of finding the focus by the Adaptive Squared Gradient Algorithm; Section 3 explains the experimental setup, and Section 4 presents the conclusions.

2. **Finding the Focus by the Adaptive Squared Gradient Algorithm.**

2.1. **Optical focusing system.**

As it is well known, perfect focus is possible at a distance where a point object forms a point image [15,16]. In Figure 1, the focal plane of a digital

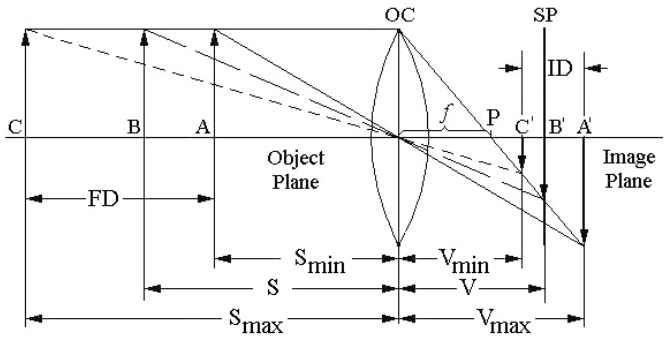

FIGURE 1. Focal plane of a digital camera with a convex lens

camera with a convex lens and an image formed on the *sensor plane* (*SP*) of an object located on the focal plane are shown.

In order to get a normal image of an object, the distance S between the object and the optic center (OC) and the distance V between SP and OC are determined by the conditions $S_{\min} \leq S \leq S_{\max}$ and $V_{\min} \leq V \leq V_{\max}$, respectively [14,15,17]. According to the Gaussian lens law, the optimum value (V_{opt}) of V providing to take a sharp image is determined by Formula (1) given below [1,4].

$$V_{opt} = \frac{S \times f}{S - f} \tag{1}$$

where f is the focus distance of the lens. Additionally, in order to obtain the sharp image, Formula (1) must provide the following condition:

$$|V - V_{opt}| \approx 0 \tag{2}$$

As it is known, this condition can only be satisfied when the focus value (FV), obtained from autofocusing algorithm by processing of the image of the object, is maximum [1,4,5,11]. In the following sections, one of the methods of reaching this goal for thermal images is elaborated on.

2.2. **The adaptive squared gradient algorithm.** As mentioned above, among autofocusing algorithms developed for visible image devices, the most appropriate one for thermal image devices is the SGA. Based on Formula (3), this algorithm determines the focus value (FV_{SGA}) by calculating the mean squared differences of adjacent pixels along the horizontal and vertical axes of the image [6,9,10,13].

$$FV_{SGA} = \frac{1}{n \times m} \sum_{i=1}^{n} \sum_{j=1}^{m} (g_{i+1,j} - g_{i,j})^2 + (g_{i,j+1} - g_{i,j})^2 \tag{3}$$

where n and m are the vertical and horizontal dimensions of the image, respectively; $g_{i,j}$ is the gray level of the pixel at coordinates $i \in \{1, 2, \ldots, n\}$ and $j \in \{1, 2, \ldots, m\}$ of the image.

It should be noted that all autofocusing algorithms including the SGA expressed by the Formula (3) obtain the differences between the gray levels of the pixels of the neighboring distance of 1. The application of the SGA to 500 different fields of the different thermal images with resolution of 480×720 showed that the average success rate of this algorithm is approximately 87%. However, as seen in Figure 2, the differences between the gray levels of the neighboring pixels decrease with the increase in the resolution of the thermal images. In the other words, the detection of mentioned differences becomes more and more difficult as the resolution of the thermal images increases. This event leads to decreasing the autofocusing success rate of the SGA for high-resolution thermal images. On the other

FIGURE 2. The distribution of the pixels of the edges in the field determined from the same thermal image taken at different resolutions

hand, use of the neighboring pixels that are further away from each other can also lead to errors in the detection of the edges of the image. This is to say that we have to rewrite Formula (3) as Formula (4) given below and find such a value for the gap k between the neighboring pixels that leads to the maximum of the focus value at the given resolution of the thermal image.

$$FV_{ASGA} = \frac{1}{n \times m} \sum_{i=1}^{n} \sum_{j=1}^{m} (g_{i+k,j} - g_{i,j})^2 + (g_{i,j+k} - g_{i,j})^2 \tag{4}$$

where k is the gap between neighboring pixels and FV_{ASGA} is the focus value. We call the SGA improved by this way as the Adaptive SGA (ASGA).

Since an analytical solution of Formula (4) does not exist, the range of the possible values for k providing the maximum value of FV_{ASGA} could only be determined experimentally. For this purpose, the value of k was experimentally obtained for all 500 different images at each of the 8 standard resolutions: 60×80, 120×160, 240×320, 480×640, 480×720, 768×1024, 960×1200 and 1200×1600. The analysis of the obtained results shows that, at each resolution, the maximal value for the FV_{ASGA} is provided at a single value of k only. The values of k associated with the resolutions of the thermal images are shown in Figure 3. As seen in this figure, k is to be equal to 1 for resolutions from 60×80 to 240×320. That is, in Formula (4), for resolutions from 60×80 to 240×320, $k = 1$ is to be used. As seen in the same figure, for the widely used resolutions from 480×640 to 480×720, $k = 2$ is taken in Formula (4). Figure 3 illustrates that for resolutions from 768×1024 to 960×1200 and for resolution 1200×1600, the gaps between the neighboring pixels must be $k = 3$ and $k = 4$, respectively. The autofocusing success rates of the ASGA reached by using different values of k for different resolutions are given in Table 1.

While the values given in the first row of Table 1 are common for the SGA and ASGA, the values in other rows belong to the ASGA only. The comparison of success rates of the SGA and ASGA is shown more clearly in Table 2.

As seen in Table 2, the highest focusing successes of the ASGA for different resolutions are obtained at different values of k. As it is seen in Table 2, beginning from the resolution

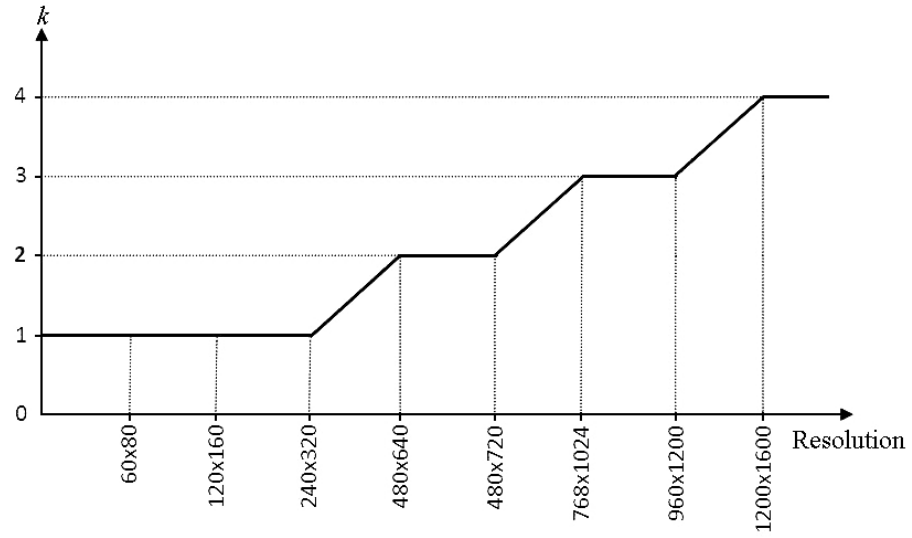

FIGURE 3. The dependency of the value of k on the resolution of the images

TABLE 1. The autofocusing success rate of the ASGA for different values of k at different resolutions

k	*The percentages of the success for different resolutions*							
	60×80	*120×160*	*240×320*	*480×640*	*480×720*	*768×1024*	*960×1280*	*1200×1600*
1	*82*	*86*	*87*	*84*	*87*	*85*	*85*	*87*
2	*67*	*84*	*85*	*91*	*92*	*87*	*87*	*88*
3	*53*	*82*	*86*	*88*	*88*	*92*	*92*	*91*
4	*35*	*72*	*85*	*85*	*87*	*88*	*88*	*96*
5	*10*	*62*	*86*	*85*	*85*	*88*	*87*	*91*

TABLE 2. The comparison of the success percentage of the SGA and ASGA

Resolution	*60×80*	*120×160*	*240×320*	*480×640*	*480×720*	*768×1024*	*960×1280*	*1200×1600*
Success rate for the SGA ($k = 1$)	*82*	*86*	*87*	*84*	*87*	*85*	*85*	*87*
Success rate for the ASGA	*82* ($k = 1$)	*86* ($k = 1$)	*87* ($k = 1$)	*91* ($k = 2$)	*92* ($k = 2$)	*92* ($k = 3$)	*92* ($k = 3$)	*96* ($k = 4$)

TABLE 3. The values of k to be selected for different resolutions

Resolution	*60×80*	*120×160*	*240×320*	*480×640*	*480×720*	*768×1024*	*960×1280*	*1200×1600*
k	*1*	*1*	*1*	*2*	*2*	*3*	*3*	*4*

480×640, the increase in the value of k significantly affects the focusing success of the ASGA. For instance, as it is seen from Table 2, while the success rate of the SGA for the resolution 1200×1600 is 87%, the success rate of the ASGA with $k = 4$ is to 96%.

Table 3, prepared based on Table 2, exhibits the values of k to be chosen for providing the highest autofocusing success of the ASGA.

In order to theoretically verify the results given in Table 3, we calculated the *Mean Squared Error (MSE)* of the focusing performed by the ASGA. For this aim, we use the

formula,

$$MSE = \frac{1}{N}\sum_{y=1}^{N}(ta_y - td_y)^2 \tag{5}$$

where ta is the real focus point of the object, td is the focus point found by the ASGA for the same object, and N is the total number of the thermal images taken. The results of calculations of Formula (5) show that depending on the resolution of the camera the minimum focusing error is provided at the following values of k.

- For the resolutions from 60×80 to 240×320 at $k = 1$;
- For the resolutions from 480×640 to 480×720 at $k = 2$;
- For the resolutions from 768×1024 to 960×1280 at $k = 3$;
- For the resolution 1200×1600 at $k = 4$.

As it is easy to see, this result is the same as that given in Table 3.

3. **The Experimental Setup.** In this study, to obtain the thermal images, a manual focus *FLIR E45* thermal camera possessing uncooled Microbolometer *Focal Plane Array* (FPA) detectors with a spectral interval of 7.5-13μm was used. The other parameters of the thermal camera are: 0.1°C thermal sensitivity at 30°C, the standard composite video signal output, 120×160 pixels and operating temperature range from 0°C to +250°C.

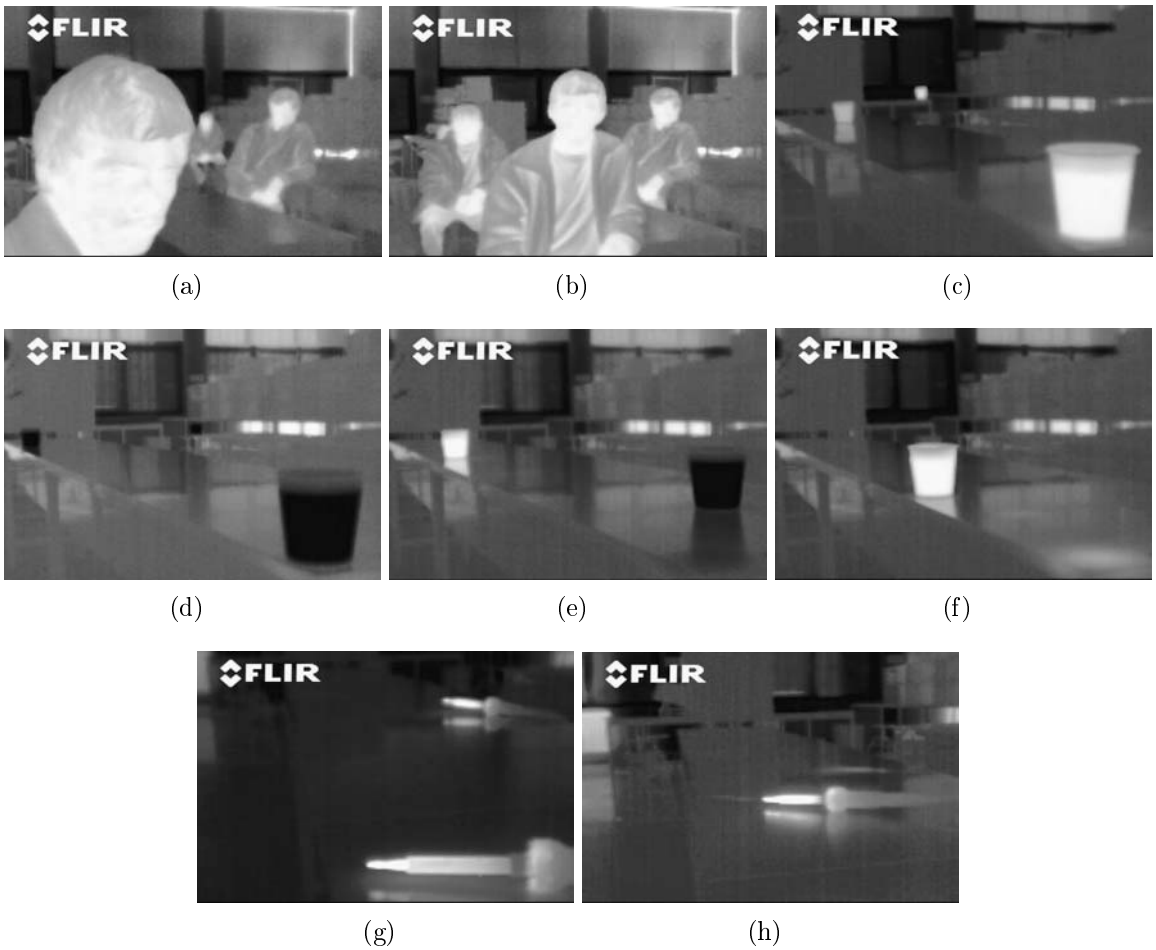

FIGURE 4. The examples of thermal images used for the tests: the human images ((a) and (b)), the images of paper cups containing hot and cold liquids ((c), (d), (e) and (f)), the hot soldering iron images ((g) and (h))

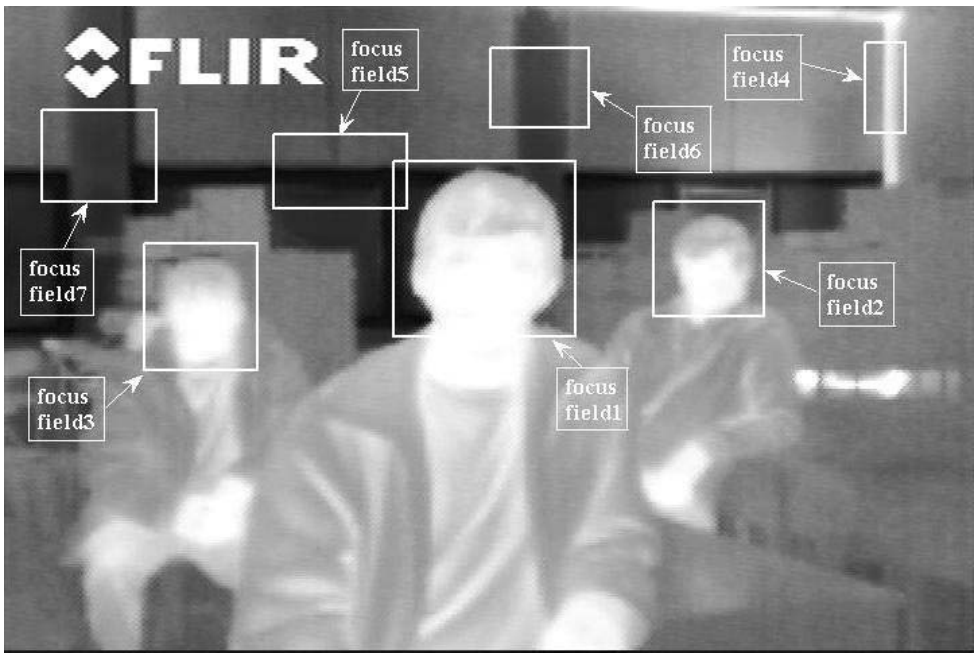

FIGURE 5. Examples of fields determined on the thermal images

For practical applicability of this study, the thermal images were taken from mediums with objects of various geometries and distances from the camera. As shown in Figure 4, these images are comprised of humans (Figures 4(a) and 4(b)), paper cups containing hot and cold liquids (Figures 4(c)-4(f)) and hot soldering irons (Figures 4(g) and 4(h)). For the experiments with thermal camera, 500 fields on different thermal images were determined. Some of these fields are shown in Figure 5 as examples. In order to obtain the success rate of each algorithm for the same image, the image fields were processed by different autofocusing algorithms. Based on these results, the success rates for each algorithm were determined (Table 4).

In this study, to determine the focal position providing to obtain the best image of a given field of thermal image at hand, the images of this field are sequentially taken starting from the distance $V_{\min}$ towards $V_{\max}$ (Figure 6). For each image taken at the point t, the FV_t is calculated using Formula (4). In this case, FV_t will continue to rise until $V \approx V_{opt}$, and then begin to fall at the instant $V > V_{opt}$. The process of taking the image is sustained until reaching the point where $FV_t < FV_{t-1}$ and focusing with respect to FV_{t-1} is deemed as the optimal one. Here, $t = 1, 2, \ldots, L$, and L is the maximum possible number of points at which images can be taken.

In order to realize the autofocusing method described above, the distance ID between $V_{\max}$ and $V_{\min}$ is divided into L steps (Figure 6) and at each step one image is taken. If the optimal number of these steps is L_{opt}, then $L < L_{opt}$ would cause to take images less than

TABLE 4. Success rates of different autofocusing algorithms

Autofocusing Method	*Total Number of Autofocus Tests*	*Total Number of Correct Autofocusing*	*Correct Autofocusing Percentage*
SGA	*500*	*435*	*87*
BA	*500*	*420*	*84*
VA	*500*	*335*	*67*
AA	*500*	*165*	*33*

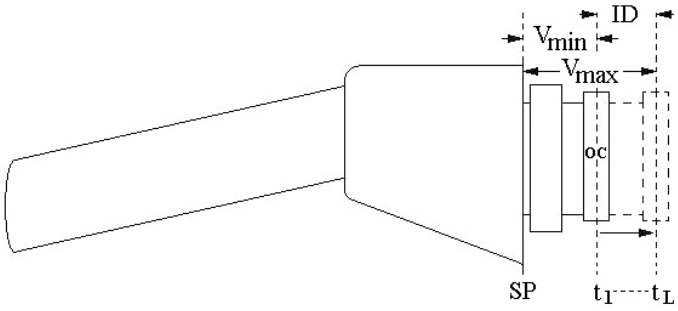

FIGURE 6. Image depth (ID) of the thermal camera

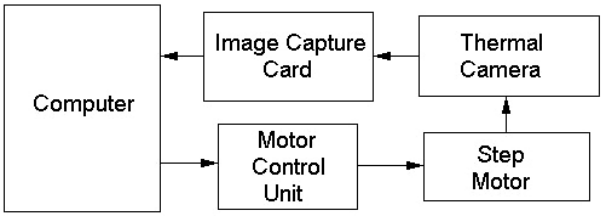

(a)

(b)

FIGURE 7. The experimental setup's diagram (a) and picture (b)

required and lead to incorrect finding of the focal position. Conversely, using $L > L_{opt}$ would cause to take images more than required and lead to superfluous consumption of memory and time. In this context, since no analytical methods exist for maintaining the condition of $L = L_{opt}$, the image depth of the thermal camera given by $ID = V_{\max} - V_{\min}$ (Figure 6), was divided into $L = 60$, 70, 80, 90 and 100 steps, and at each of them one image was taken. By comparing the sharpness of these images, we concluded that it is impossible to get a good image when $L < 90$. On the other hand, the sharpness of an image reached its maximum at L closed to 100. Therefore, to move the objective of the thermal camera, we used a step motor mechanism passing the distance $ID = V_{\max} - V_{\min}$ at $L = 100$ steps.

The experimental setup required for the autofocusing of thermal camera used in this study is given in Figures 7(a) and 7(b).

4. **Conclusions.** In this study, the AA, VA, BA, SGA algorithms that are commonly used for autofocusing in digital imaging devices were applied to 500 different fields determined on different thermal images. For each algorithm, the autofocusing success rate was recorded. According to the results obtained, among these algorithms currently in use, the most convenient one to be used in thermal imaging is the SGA. We observed that the quality of a thermal image taken is significantly affected by the resolution of the camera used and by the gap between the neighboring pixels. Therefore, we improved the SGA so that it uses such a gap between the neighboring pixels that is best for resolution of an image being processed. This approach denominated as *Adaptive Squared Gradient Algorithm* (ASGA) improved the autofocusing success of the SGA from 87% to 96%.

Acknowledgement. This work is supported by Selçuk University Scientific Research Projects Coordinatorship, Konya, Turkey.

REFERENCES

[1] C. Y. Chen, R. C. Hwang and Y. J. Chen, A passive auto-focus camera control system, *Applied Soft Computing*, vol.10, no.1, pp.296-303, 2010.

[2] H. C. Chang, T. M. Shih, N. Z. Chen and N. W. Pu, A microscope system based on bevel-axial method auto-focus, *Optics and Lasers in Engineering*, vol.47, no.5, pp.547-551, 2009.

[3] S. Wu, W. Lin, L. Jiang, W. Xiong, L. Chen and S. H. Ong, An objective out-of-focus blur measurement, *The 5th Int. Con. on Information Communications and Signal Processing*, pp.334-338, 2005.

[4] Y. Zhang, Y. Zhang and C. Y. Wen, A new focus measure method using moments, *Image and Vision Computing*, vol.18, no.12, pp.959-965, 2000.

[5] S. H. Jin, J. U. Cho and J. W. Jeon, FPGA based passive auto focus system using adaptive thresholding, *SICE-ICASE Int. Con.*, pp.2290-2295, 2006.

[6] Q. Wu, F. A. Merchant and K. R. Castleman, *Microscope Image Processing*, Academic Press, USA, 2008.

[7] Y. Liron, Y. Paran, N. G. Zatorsky, B. G. Geiger and Z. Kam, Laser autofocusing system for high-resolution cell biological imaging, *Journal of Microscopy*, vol.221, no.2, pp.145-151, 2006.

[8] J. H. Price and D. A. Gough, Comparison of phase-contrast and fluorescence digital autofocus for scanning microscopy, *Cytometry*, vol.16, no.4, pp.283-297, 1994.

[9] W. Huang and Z. Jing, Evaluation of focus measures in multi-focus image fusion, *Pattern Recognition Letters*, vol.28, no.4, pp.493-500, 2007.

[10] P. Liatsis and P. Kantartzis, Real-time colour segmentation and autofocus in retinal images, *The 47th Int. Sym. ELMAR Multimedia Systems and Applications*, pp.13-18, 2005.

[11] Y. Sun, S. Duthaler and B. J. Nelson, Autofocusing algorithm selection in computer microscopy, *Int. Con. on Intelligent Robots and Systems (IROS)*, pp.419-425, 2005.

[12] A. Santos, C. O. De Solorzano, J. Vaquero, J. M. Pena, N. Malpica and F. Del Pozo, Evaluation of autofocus functions in molecular cytogenetic analysis, *Journal of Microscopy*, vol.188, no.3, pp.264-272, 1997.

[13] F. Groen, I. T. Young and G. Ligthart, A comparison of different focus functions for use in autofocus algorithms, *Cytometry*, vol.6, no.2, pp.81-91, 1985.

[14] M. Subbarao and J. K. Tyan, The optimal focus measure for passive autofocusing and depth-from-focus, *The Int. Soc. for Optics and Photonics (SPIE)*, vol.2598, pp.89-99, 1995.

[15] R. E. Jacobson, S. F. Ray, G. G. Atteridge and N. R. Axford, *The Manual of Photography: Photographic and Digital Imaging*, Focal Press, Great Britain, 2000.

[16] N. Salvaggio, L. Stroebel and R. D. Zakia, *Basic Photographic Materials and Processes*, Focal Press, China, 2008.

[17] S. F. Ray, *Applied Photographic Optics*, Focal Press, Great Britain, 2002.